Configuration-interaction projected density functional theory: Effects of four-quasiparticle configurations and time-odd interactions

Yi Li (李义)

School of Physics and Astronomy, Sun Yat-Sen University

Journal Club (20251210)

Reference: Y. K. Wang et al., PRC 105, 054311 (2022)

Abstract

Configuration-interaction projected density functional theory: Effects of four-quasiparticle configurations and time-odd interactions

Y. K. Wang, P. W. Zhao,* and J. Meng†

State Key Laboratory of Nuclear Physics and Technology, School of Physics, Peking University, Beijing 100871, China

(Received 10 April 2022; accepted 2 May 2022; published 16 May 2022)

The effects of four-quasiparticle configurations and time-odd interactions are investigated in the framework of configuration-interaction projected density functional theory by taking the yrast states of ^{60}Fe as examples. Based on the universal PC-PK1 density functional, the energies of the yrast states with spin up to $20\hbar$ and the available $B(E2)$ transition probabilities are well reproduced. The yrast states are predicted to be of four-quasiparticle structure above spin $I = 16\hbar$. The inclusion of the time-odd interactions increases the kinetic moments of inertia and delays the appearance of the first band crossing, and, thus, improves the description of the data.

DOI: 10.1103/PhysRevC.105.054311

Introduction

The nuclear DFT is based on the idea that the ground-state energy of a nucleus can be expressed as a functional of the nucleon density.

$$\begin{aligned}\mathcal{E}^{\text{int}}(\boldsymbol{r}) = &\frac{\alpha_S}{2}\rho_S^2 + \frac{\beta_S}{3}\rho_S^3 + \frac{\gamma_S}{4}\rho_S^4 + \frac{\delta_S}{2}\rho_S\triangle\rho_S \\ &+ \frac{\alpha_V}{2}j_\mu j^\mu + \frac{\gamma_V}{4}(j_\mu j^\mu)^2 + \frac{\delta_V}{2}j_\mu\triangle j^\mu \\ &+ \frac{\alpha_{TV}}{2}\vec{j}^{\,\mu}_{TV}\cdot(\vec{j}_{TV})_\mu + \frac{\delta_{TV}}{2}\vec{j}^{\,\mu}_{TV}\cdot\triangle(\vec{j}_{TV})_\mu,\end{aligned}$$

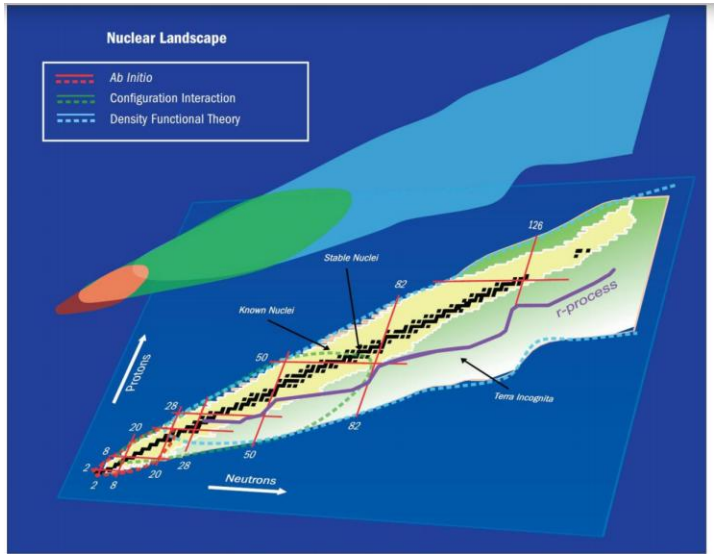

- applicable for nuclei all over the nuclide chart.
- takes into account many-body correlations by breaking essential symmetries
- describes fruitful physics around the minima of the potential energy surface.

"However, the nuclear DFT is limited to **describe nuclear ground states**. For quantitative investigations of **nuclear spectroscopic properties**, one needs to resort to proper extensions based on the DFT."

Introduction

- GCM:
  - Nonrelativistic DFTs:
    A. Valor, et al., Nucl. Phys. A 671, 145 (2000)
    R. Rodríguez-Guzmán, et al., Nucl. Phys. A 709, 201 (2002)
    M. Bender, et al., Phys. Rev. C 73, 034322 (2006)
  - Relativistic DFTs:
    T. Nikšić, et al., Phys. Rev. C 73, 034308 (2006)

Successes in :
- Shape coexistence
- Erosion of shell-closure
- collective band structures of superheavy nuclei
- novel modes of nuclear weak decays

"DFT-based GCM approaches **are limited to describe spectra with energies below the first two-quasiparticle excitations**"

- Cranking models
  - Nonrelativistic DFTs:
    J. L. Egido and L. M. Robledo, Phys. Rev. Lett. 70, 2876 (1993)
    W. Satuła and R. A. Wyss, Rep. Prog. Phys. 68, 131 (2005)
  - Relativistic DFTs:
    D. Vretenar, et al., Phys. Rep. 409, 101 (2005)
    J. Meng, et al., Front. Phys. 8, 55 (2013)
  - Two- and three-dimension tilted axis cranking DFTs
    P. Olbratowski, J. Dobaczewski, J. Dudek, and W. Płóciennik, Phys. Rev. Lett. 93, 052501 (2004).
    P. W. Zhao, J. Peng, H. Z. Liang, P. Ring, and J. Meng, Phys. Rev. Lett. 107, 122501 (2011).
    P. W. Zhao, Phys. Lett. B 773, 1 (2017).

Successes in :
- spectra with higher excitation energies
- many novel rotational phenomena

"However, the **band crossing phenomena cannot be properly described** by the cranking approach because the cranking states are obtained at a constant rotational frequency rather than a constant angular momentum."

This work

- CI-PDFT(configuration-interaction projected density functional theory):
  - **Proposed in**: *P. W. Zhao, P. Ring, and J. Meng, Phys. Rev. C 94, 041301(R) (2016),* ***two*-quasiparticle**
  - **Configuration space**: its dimension is much smaller than that in the traditional shell models.
  - **Advantages:**
    1) requires no parameters beyond those of the density functional
    2) efficiently describe detailed spectroscopic features up to high spin.

"In the present work, the CI-PDFT including contributions from the **four-quasiparticle configurations** and **time-odd interactions** is developed."

Theoretical framework

EDF

$$\begin{aligned}\mathcal{L} &= \bar{\psi}(i\gamma_\mu\partial^\mu - m)\psi \\ &- \frac{1}{2}\alpha_S(\bar{\psi}\psi)(\bar{\psi}\psi) - \frac{1}{2}\alpha_V(\bar{\psi}\gamma_\mu\psi)(\bar{\psi}\gamma^\mu\psi) \\ &- \frac{1}{2}\alpha_{TV}(\bar{\psi}\vec{\tau}\gamma_\mu\psi)(\bar{\psi}\vec{\tau}\gamma^\mu\psi) \\ &- \frac{1}{3}\beta_S(\bar{\psi}\psi)^3 - \frac{1}{4}\gamma_S(\bar{\psi}\psi)^4 - \frac{1}{4}\gamma_V[(\bar{\psi}\gamma_\mu\psi)(\bar{\psi}\gamma^\mu\psi)]^2 \\ &- \frac{1}{2}\delta_S\partial_\nu(\bar{\psi}\psi)\partial^\nu(\bar{\psi}\psi) - \frac{1}{2}\delta_V\partial_\nu(\bar{\psi}\gamma_\mu\psi)\partial^\nu(\bar{\psi}\gamma^\mu\psi) \\ &- \frac{1}{2}\delta_{TV}\partial_\nu(\bar{\psi}\vec{\tau}\gamma_\mu\psi)\partial^\nu(\bar{\psi}\vec{\tau}\gamma^\mu\psi) \\ &- \frac{1}{4}F^{\mu\nu}F_{\mu\nu} - e\frac{1-\tau_3}{2}\bar{\psi}\gamma^\mu\psi A_\mu,\end{aligned}$$

RHB equation

$$\begin{pmatrix}\hat{h}_D - \lambda & \hat{\Delta} \\ -\hat{\Delta}^* & -\hat{h}_D^* + \lambda\end{pmatrix}\begin{pmatrix}U_k \\ V_k\end{pmatrix} = E_k\begin{pmatrix}U_k \\ V_k\end{pmatrix}$$

$$\hat{h}_D = \boldsymbol{\alpha}\cdot(\boldsymbol{p} - \boldsymbol{V}) + \beta(m + S) + V,$$

$$\Delta_{ab} = \frac{1}{2}\sum_{c,d}\langle ab|V^{pp}|cd\rangle_a\kappa_{cd}$$

V^{pp} is chosen as the finite –range separable force.

$$V(\mathbf{r}_1, \mathbf{r}_2, \mathbf{r}_1', \mathbf{r}_2') = -G\delta(\mathbf{R} - \mathbf{R}')P(r)P(r')\frac{1}{2}(1 - P^\sigma)$$

Y. Tian, Z. Y. Ma, and P. Ring, Phys. Lett. B 676, 44 (2009)

CI-CDFT

Configuration space:

$$\{|\Phi_0\rangle, \hat{\beta}_{\nu_i}^\dagger\hat{\beta}_{\nu_j}^\dagger|\Phi_0\rangle, \hat{\beta}_{\pi_i}^\dagger\hat{\beta}_{\pi_j}^\dagger|\Phi_0\rangle, \hat{\beta}_{\nu_i}^\dagger\hat{\beta}_{\nu_j}^\dagger\hat{\beta}_{\pi_k}^\dagger\hat{\beta}_{\pi_l}^\dagger|\Phi_0\rangle$$
$$\hat{\beta}_{\pi_i}^\dagger\hat{\beta}_{\pi_j}^\dagger\hat{\beta}_{\pi_k}^\dagger\hat{\beta}_{\pi_l}^\dagger|\Phi_0\rangle, \hat{\beta}_{\nu_i}^\dagger\hat{\beta}_{\nu_j}^\dagger\hat{\beta}_{\nu_k}^\dagger\hat{\beta}_{\nu_l}^\dagger|\Phi_0\rangle\}.$$

The wave function in laboratory frame:

$$|\Psi_{IM}^\sigma\rangle = \sum_\eta F_\eta^{I\sigma}\hat{P}_{MK}^I|\Phi_\eta\rangle$$

The expansion coefficients $F_\eta^{i\sigma}$ are determined by solving the eigenvalue equation:

$$\sum_{\eta'}[H_{\eta\eta'}^I - E^{I\sigma}N_{\eta\eta'}^I]F_{\eta'}^{I\sigma} = 0$$

$$H_{\eta\eta'}^I = \langle\Phi_\eta|\hat{H}\hat{P}_{KK'}^I|\Phi_{\eta'}\rangle, \quad N_{\eta\eta'}^I = \langle\Phi_\eta|\hat{P}_{KK'}^I|\Phi_{\eta'}\rangle$$

Numerical details

- **Force :** PC-PK1
- **Pairing:** finite-range separable force + pairing strength $\mathrm{G} = 728\ \mathrm{MeVfm}^3$
- **Basis:** three-dimensional harmonic oscillator basis in Cartesian coordinates with $N_f = 10$ major shells
- **Configuration space**: 0, 2, and 4-qp states
  (For simplicity, four like-nucleon configurations are not included.)

Results

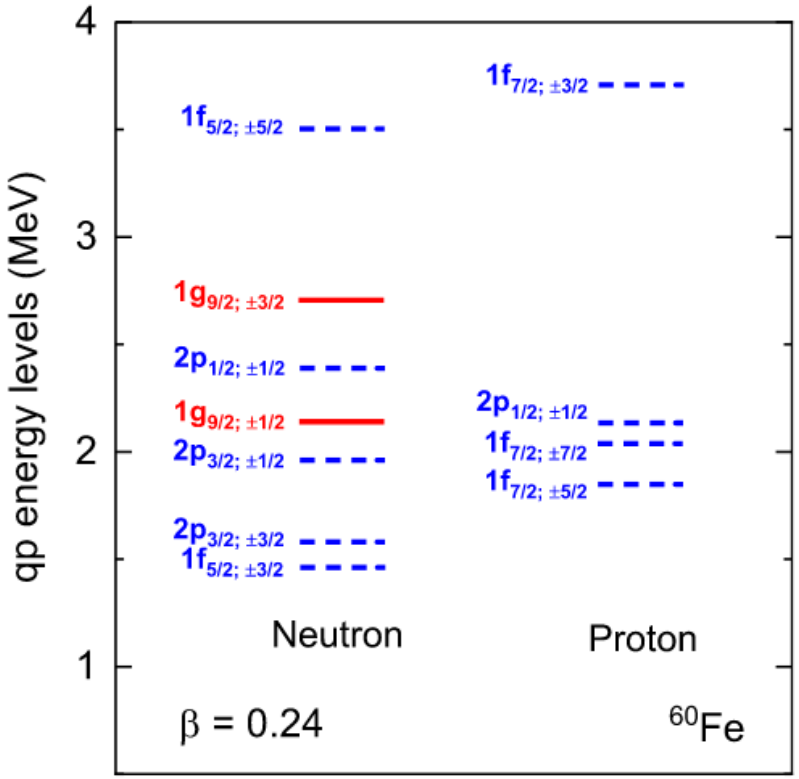

FIG. 1. The neutron and proton qp energy levels of ^{60}Fe. The qp energy levels with positive and negative parities are denoted respectively by solid and dashed lines. The approximate spherical quantum numbers are used to label the qp energy levels (see text).

- Due to the time-reversal symmetry, the qp energy levels are twofold degenerate

The dimension of the configuration space is truncated with a qp excitation energy cutoff E_{cut}

- For two-qp states: E_{cut}= **5.0 MeV**, **30 states** = 21 (neutron) + 9 (proton)
- For four-qp states: only the ones with two $g_{9/2}$ neutrons are considered, **27 states**

Total: 58 = 1 + 30 + 27

Results

band diagram

$$E_\eta(I) = \frac{\langle \Phi_\eta | \hat{H} \hat{P}^I_{KK} | \Phi_\eta \rangle}{\langle \Phi_\eta | \hat{P}^I_{KK} | \Phi_\eta \rangle}$$

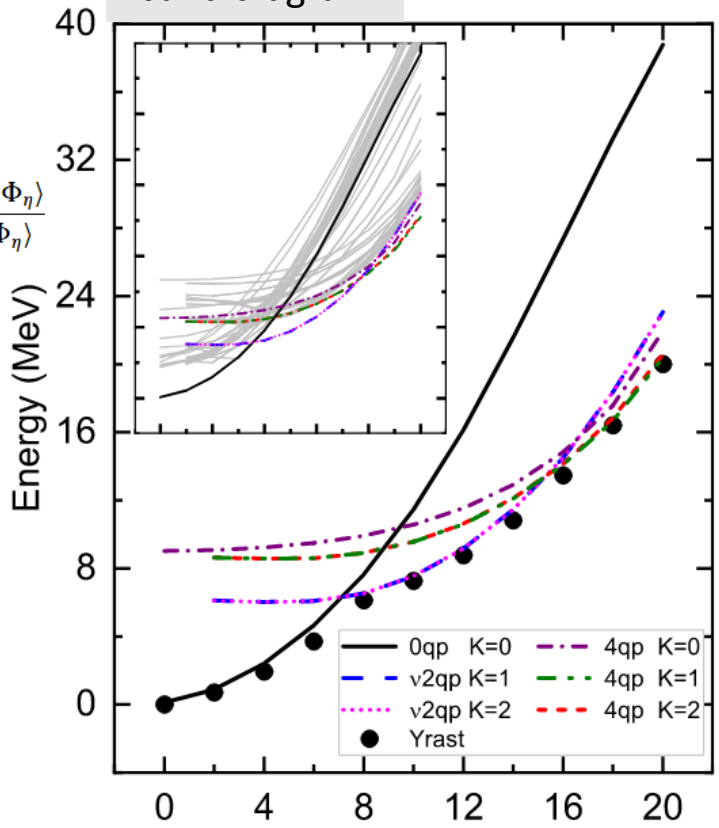

ν2qp,K=1 $\nu(g_{9/2,-1/2})^1(g_{9/2,3/2})^1$

ν2qp,K=2 $\nu(g_{9/2,1/2})^1(g_{9/2,3/2})^1$

4qp,K=0 $\nu(g_{9/2,-1/2})^1(g_{9/2,1/2})^1 \otimes \pi(p_{1/2,1/2})^1(p_{1/2,-1/2})^1$

4qp,K=1 $\nu(g_{9/2,-1/2})^1(g_{9/2,3/2})^1 \otimes \pi(p_{1/2,1/2})^1(p_{1/2,-1/2})^1$

4qp,K=2 $\nu(g_{9/2,1/2})^1(g_{9/2,3/2})^1 \otimes \pi(p_{1/2,1/2})^1(p_{1/2,-1/2})^1$

- The band diagram provides useful information for understanding the structure changes even before the diagonalization is carried out.
- The energy of the 0qp band with K = 0 increases with spin and the band quickly enters into the high energy region, thus becoming unfavored for the states in the high spin region.
- In contrast, the $\nu 2$qp bands with K = 1 and K = 2 show first a constant dependence with spin, and then cross the 0qp band at $I = 8\hbar$. This behavior makes the two-qp states with two $g_{9/2}$ neutrons the most important configurations for the spin interval $I = 8\text{–}14\ \hbar$.
- The $\nu 2$qp bands become less favorable above $I = 14\ \hbar$, and the 4qp bands with K = 0, K = 1, and K = 2 cross them and become more important.

Results

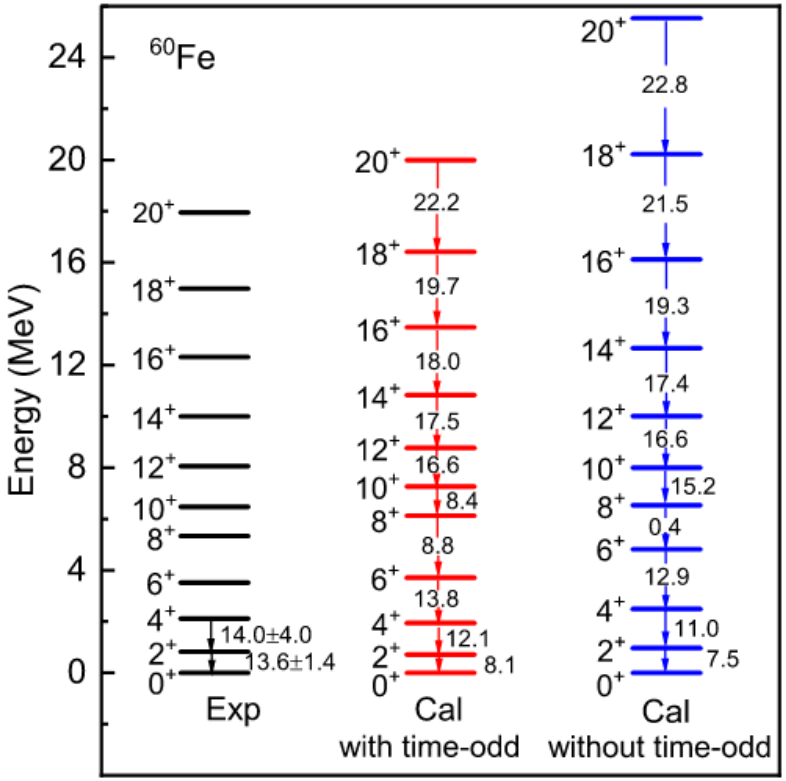

- It is found that the energy levels as well as the E2 transition probabilities calculated by the CI-PDFT with time-odd interactions agree well with the available data.
- In particular, the irregularity shown in the energy levels, i.e., the compressed levels spacings, at around $I = 8\hbar$ is also reproduced satisfactorily.
- The irregularity is mainly caused by the band crossing between the $\nu 2\mathrm{qp}$ neutron bands with $K = 1, 2$ and the 0qp band with $K = 0$.

Results

$$G_{\eta}^{I\sigma} = \sum_{\eta'} (N^{I})_{\eta\eta'}^{1/2} F_{\eta'}^{I\sigma}$$

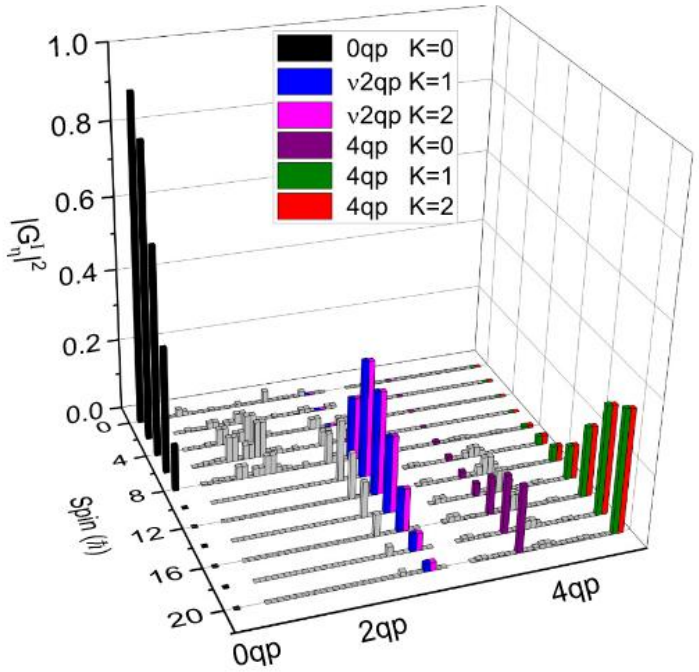

- 0qp state plays dominant roles for the yrast states with $I \leq 6\hbar$. The corresponding probability amplitude $\left|G_{\eta}^{I\sigma}\right|^2$ decreases gradually with spin.

- The $\left|G_{\eta}^{I\sigma}\right|^2$ of the $\nu 2$qp neutron states with K = 1 and 2 increase suddenly at $I = 8\hbar$, which is consistent with the drop observed in the B(E2) value at around I = 8h.

- The 4qp states win after $I = 16\hbar$, and the yrast states are predicted to be of 4qp structure.

Results

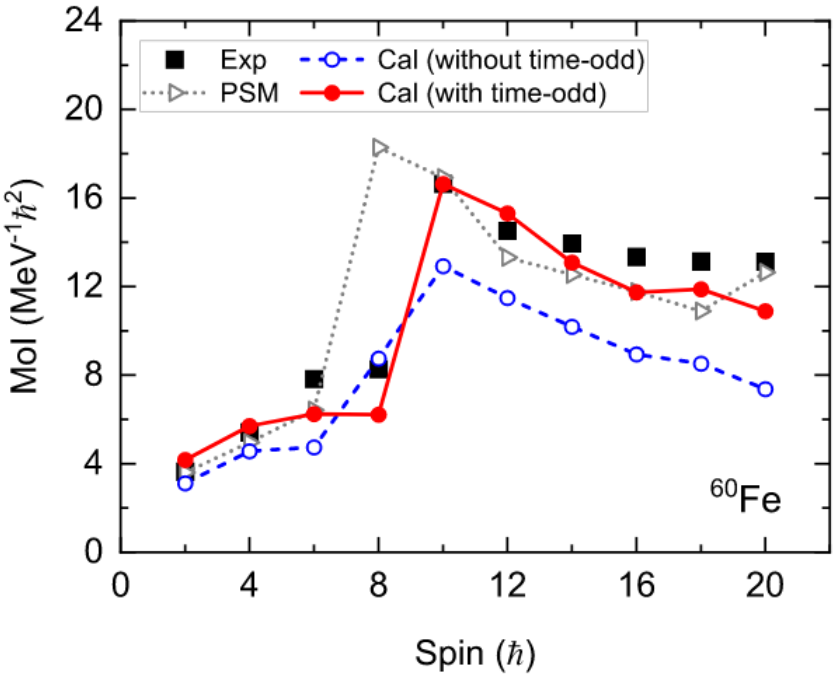

- The energies of yrast states are overestimated by the CI-PDFT calculations without time-odd interactions originate from the underestimation of the moments of inertia.
- MOI calculated without time-odd interactions **underestimate** the data, especially for the ones with $I \geq 10\hbar$.
- A sharp increase of MOI occurs at $I = 6\hbar$ for both of the PSM calculations and the CI-PDFT ones without time-odd interactions. This **disagrees** with the experimental observation
- The inclusion of time-odd interactions predicts larger MOI and delays the appearance of the band crossing and achieves **better** descriptions of the data.

Summary

- The study investigates the effects of four-quasiparticle configurations and time-odd interactions within the CI-PDFT framework, using the yrast states of $^{60}\mathrm{Fe}$ as examples.
- The energies and the B(E2) transition probabilities of the yrast states are well reproduced.
- Analysis of angular momentum projected states and the probability amplitudes for some important quasiparticle configurations, the dominant roles of the neutron $g_{9/2}$ orbits are emphasized and a weak band crossing caused by the four-quasiparticle configurations at around $I = 14\ \hbar$ is also predicted.
- It is found that the inclusion of the time-odd interactions could increase the kinetic moments of inertia and delay the appearance of first band crossing observed in $^{60}\mathrm{Fe}$.